Nano-Structures & Nano-Objects 34 (2023) 100956

Contents lists available at ScienceDirect

Nano-Structures & Nano-Objects

journal homepage: www.elsevier.com/locate/nanoso

Low-cost, mass-producible nanostructured surface on flexible substrate with ultra-thin gold or silver film for SERS applications

Emil Rosqvist [a], Ulrike Böcker [b], Tina Gulin-Sarfraz [b], Nils Kristian Afseth [b], Stiina Tolvanen [a], Jouko Peltonen [a], Jawad Sarfraz [b,*]

[a] Physical Chemistry, Laboratory of Molecular Science and Engineering, Åbo Akademi University, Henriksgatan 2, FI-20500 Åbo, Finland
[b] Nofima-Norwegian Institute of Food, Fisheries and Aquaculture Research, P.O. Box 210, NO-1431, Ås, Norway

ARTICLE INFO

Article history:
Received 7 July 2022
Received in revised form 5 January 2023
Accepted 17 February 2023

Keywords:
SERS
Paper
Low-cost
Disposable
Roll-to-roll
Nanostructure

ABSTRACT

Surface Enhanced Raman Spectroscopy has emerged as a powerful analytical technique for fingerprint recognition of molecular samples with high sensitivity. The Surface Enhanced Raman Scattering (SERS) effect has been extensively studied for the past few decades. However, only recently the commercialization of portable Raman spectrometers has taken SERS a step closer to real-world applications. Swift and convenient testing of analytes for point-of-care, environmental as well as food quality control and safety applications, is very lucrative. This can be realized with the use of low-cost, mass producible and environmentally friendly SERS active substrates in combination with portable Raman spectrometers. In this study, we demonstrate one approach to accomplish such a SERS-active substrate using nanostructured latex coated paperboard as a base substrate. The nanostructure is accomplished by applying a reverse gravure coater in combination with a short-wavelength infrared (IR) heater. The whole process is easily up-scalable. The SERS functionality is then obtained by physical vapor deposition of an ultra-thin layer of Au or Ag. The surface nanostructure was confirmed by atomic force microscopy, showing an additional nanoscale graininess after the deposition of Au or Ag. The successful metal deposition was confirmed by X-ray photoelectron spectroscopy and deposition homogeneity was also analyzed. To confirm the SERS effect, two model compounds; crystal violet and rhodamine 6G were tested in the concentration range of 1–1000 μM. The results confirmed that the nanostructured, flexible, paper-based substrate can perform as a SERS-active substrate with negligible background noise.

1. Introduction

In recent years, Surface-Enhanced Raman Scattering (SERS) has emerged as a powerful analytical technique. The ultra-high sensitivity combined with fingerprinting recognition capabilities of SERS enables trace level detection of the analytes [1,2]. The surface enhancement effect is mainly explained with the "localized surface plasmon resonance" and the "chemical" or "charge-transfer" mechanisms [3]. The SERS effect has been studied extensively for the past few decades. Only recently, the commercialization of portable Raman spectrometers has taken SERS a step closer to real-world applications. Such are food safety and quality control, medical diagnostics, homeland security and environmental monitoring [4].

To extend the use of SERS to real life applications, there is a need to develop low-cost environment-friendly disposable analysis chips with high accuracy and specificity, as well as to avoid the risks of cross contamination and false positives. Methods such as spin-coating, dip coating, chemical vapor deposition, electrochemical synthesis, electron beam lithography, soft lithography and etching have been reported in the literature to fabricate structured SERS-active substrates, but these methods have limitations in terms of throughput volume and/or cost [5]. Furthermore, one of the challenges with mass-producible SERS-active nanostructures is obtaining a spatial reproducibility of the signal intensity [6].

Paper is a low-cost, flexible and environment-friendly substrate. Proof-of-concepts for paper-based printed electronics [7,8] and paper-based platforms for analytical applications have been reported in the literature [9–11]. These concepts were developed by combining surface engineering methods with printing and coating technologies. However, for SERS, paper is not an ideal substrate as it can create background disturbance. Recently, we have described the use of nanostructured latex coated paper substrates in a wide range of applications. This substrate is utilized for studying adsorption of biomaterials (bacteria, proteins, cells) [12,13] as well as for the development of sensors [14,15]. Here we

* Corresponding author.
E-mail address: jawad.sarfraz@nofima.no (J. Sarfraz).

https://doi.org/10.1016/j.nanoso.2023.100956

demonstrate the SERS-active properties of said nanostructured paper substrate with an ultra-thin (as low as 2.5 nm) gold or silver layer resulting in negligible background disturbance.

2. Materials and methods

2.1. Latex coatings

The latex coating used was a 50:50 blend (by volume) of two commercial latex dispersions. One is a polystyrene (PS) dispersion (HPY83, Trinseo GmbH, CH) with a glass transition temperature (T_g) of 105 °C and an average particle size of 130 nm, and the other a polymerized acrylonitrile butadiene styrene (ABS) copolymer dispersion with an average particle size of 140 nm (HPC26, Trinseo GmbH, CH) and a T_g of 10 °C. The PS and ABS dispersions had a solids content of around 48% and 55%, respectively.

The latex blend was coated onto a commercial uncoated paperboard base produced by Billerud Korsnäs (Sweden). The 348 ± 3 μm thick board had a base weight of 272 ± 2 gm^{-2}. The coater used was a MiniLabo reverse gravure coater (Yasui Seiki Co., Japan) using a microgravure roll of 120 lines per inch and a 65 μm depth, giving an approximate wet thickness of 5–11 μm with a transfer fraction of 0.28. Coating web speed was 0.5 m min^{-1} and the gravure roll rotational speed was 25 rpm. Nanostructured surface texture was finalized by irradiating the latex coating with a short-wavelength infrared (IR) heater with 1 kW power (IRT systems, Hedson Technologies AB, Sweden). A more detailed description of the latex surface can be found in [16].

2.2. Physical vapor deposition

Silver and gold were deposited onto the nanostructured latex coated paperboard using physical vapor deposition (PVD) with electrically resistive heating. The evaporation was done under vacuum (3–6 x 10^{-6} mbar) during separate runs utilizing aluminum-coated tungsten baskets. The evaporation rate was set to 0.1 kÅ/min. The film thickness was gravimetrically determined using a deposition monitor (XTM/2, Inficon, Switzerland). Four separate samples were produced: 2.5 nm thick layer of gold and silver (Au-2.5, Ag-2.5 respectively) and 5 nm thick layer of gold and silver (Au-5, Ag-5 respectively).

2.3. Atomic force microscopy

Atomic force microscopy (AFM) was used to image the topography and characterize the surface roughness of the coatings. Measurements were done with a Nanoscope V Multimode 8 AFM (Bruker, USA), using aluminum coated ScanAsyst-Air probes with a spring constant $k = 0.4$ (0.2–0.8) N/m and a nominal tip radius of 2 nm. Images of 1 μm × 1 μm size (512 × 512 pixels) were obtained at 24±1.5 °C and 45 ± 6% relative humidity.

Image analysis was conducted using a Nanoscope Analysis software (Bruker, USA). Roughness values were calculated from the 1 μm × 1 μm topographical images. The following parameters were used for the quantification of the surfaces; the RMS roughness (S_q) being the standard deviation of surface heights, the developed surface area ratio (S_{dr}), and the density of local maxima, summits, given by the summit density parameter (S_{ds}). The 3D rendering of the surfaces was done with MountainsSPIP software (v9.2.9994, Digital Surf, France). The same roughness values were obtained with both analysis software.

2.4. X-ray photoelectron spectroscopy

X-ray photoelectron spectroscopy (XPS) spectra were obtained with a Kratos Axis Ultra^{DLD} XPS instrument using a monochromatic Al Kα X-ray source (1486.6 eV) operating at 15 kV and 10 mA at normal emission angle. For survey and high-resolution spectra, the used pass energy was 80 eV and 20 eV, respectively. XPS measurements were performed on three separate spots for each sample. XPS measurements were executed on ultra-thin gold and silver samples stored under ambient conditions for three months to examine the shelf stability of these samples. The atomic concentration (at.%) of the different elements was derived by calculating the area of the peaks and correcting for the sensitivity factors using the CasaXPS software.

2.5. SERS measurements and spectral data analysis

Crystal violet and rhodamine 6G supplied by Merck were chosen as the test analytes and measured for the following concentrations for all four substrates: 1, 10, 20, 50, 70, 100, and 1000 μM. Samples were prepared by dropping and air-drying 5 μL of analyte solution onto the substrates. Spectral acquisition was carried out with a Kaiser RXN2 system (Endress & Hauser Optical Analysis, USA) with a 785 nm laser (laser operating power of 100 mW) equipped with an MR-probe. The exposure time was set to 1 s with 5 accumulations. The spectral range was 300–1800 cm^{-1}. Spectra were collected from two analyte spots per substrate, and two spectra (from two different areas) were measured per spot. For all spectra, the fluorescence background was removed using a modified polynomial baseline fitting routine [17] employing a third order polynomial. After background removal, all spectra were normalized for the intensity of the substrate-related band at 1001 cm^{-1}. The analytical enhancement factor (AEF) was calculated according to [18] as follows: $AEF = (I_{SERS}/C_{SERS})/(I_{REF}/C_{REF})$ with I_{SERS} and I_{REF} being the peak intensity for spectra after background removal without normalization for SERS and normal Raman spectra, respectively. C_{SERS} and C_{REF} are the molar concentrations for the respective measurements. The peak intensities selected for AEF calculation were the maximum intensity found at around 1172 cm^{-1} for crystal violet and around 1360 cm^{-1} for rhodamine 6G. The maximum intensity varied slightly depending on the substrate and was chosen accordingly for each substrate. Normal Raman spectra of crystal violet and rhodamine 6G were obtained on a standard glass substrate (i.e. CaF_2).

3. Results and discussion

3.1. Atomic force microscopy

AFM images confirmed the changes of the surfaces after the different manufacturing steps. In images of the uncoated paperboard any finer details in the topography were typically overshadowed by larger fiber structures (Fig. 1a). These fibers resulted in large height variations. The topography of the latex coated paperboard (Fig. 1b) was smoother and showed a bimodal nanostructure consisting of PS particles and an interjacent smooth ABS phase. The influence of the coating on paperboard has also been described in [11]. The particles represent high-T_g PS whereas the intermittent lower and smoother phase represents ABS, which due to the low T_g had formed a film at room temperature. The composite latex film had also been IR-treated, causing annealing and flattening of the PS particles [14]. The deposited ultra-thin metal film appeared as a grainy surface (Fig. 1c–f). The nanoscale graininess is highlighted by edge effects along the contact regions of grains in the phase contrast maps (Figure S1). These are the

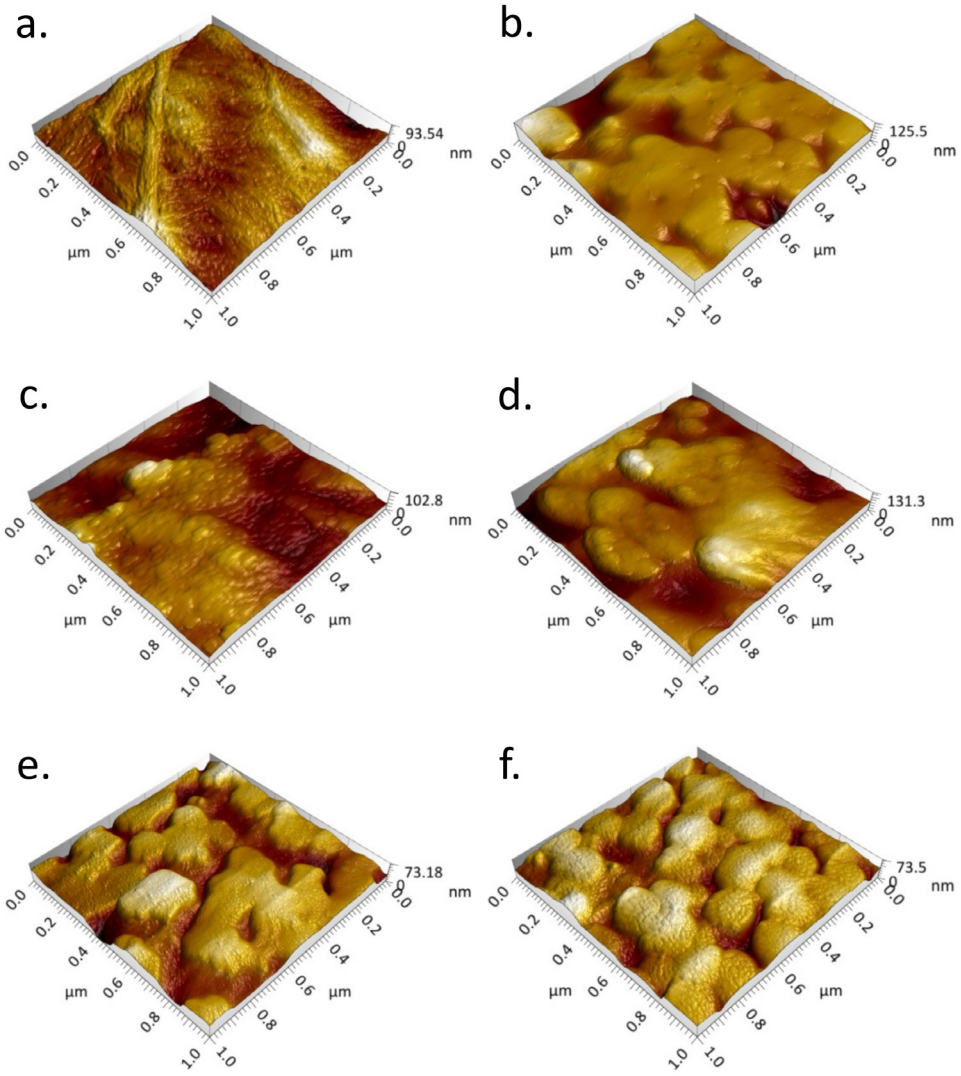

Fig. 1. Representative AFM images (1 µm × 1 µm) of (a) uncoated paperboard (Z = 93.5 nm), (b) latex coated paperboard without deposited metal (Z = 125.5 nm), (c) 2.5 nm thick vapor deposited layer of silver on nanostructured latex coated paperboard (Z = 102.8 nm), (d) 5 nm thick vapor deposited layer of silver on nanostructured latex coated paperboard (Z = 131.3 nm), (e) 2.5 nm thick vapor deposited layer of gold on nanostructured latex coated paperboard (Z = 73.2 nm), and (f) 5.0 nm thick vapor deposited layer of gold on nanostructured latex coated paperboard (Z = 73.5 nm).

nano-scale aggregates of the deposited metal, as was further confirmed by X-ray photoelectron spectroscopy (Section 3.2). It can also be seen in Fig. 1c–f that the deposited metal films follow nicely the underlying latex nanostructure. Previously, thicker layers of deposited gold were observed to infiltrate the latex structure [15].

In terms of roughness parameters, the uncoated paperboard had the largest height variations, with a S_q being 41.1 nm (Fig. 2, Table S1). The surface was also quite heterogeneous, as can be seen from the large standard deviation values. The surface of the latex coating had a relatively low S_q and S_{dr}, compared to the surfaces with metal depositions (Fig. 2, Table S1). Only the Ag-2.5 had a similar or lower S_q and S_{dr}. This increase can be attributed to the added fine structure, i.e. the 'nano-graininess', resulting from the metal depositions. Surfaces with depositions of Au were rougher than the Ag surfaces. The deposition thickness did not clearly influence the roughness of Au in terms of S_{dr} and S_{ds}. Further, comparing 2.5 nm Au to 5 nm Au depositions, S_q increased only 14%. Meanwhile, the S_q and S_{dr} values of the Ag samples were closer to those of the latex coated substrate. However, a more pronounced increase in S_q and S_{dr} was observed with increasing Ag thickness (59% for S_q and 47% for S_{dr}). The effects of depositions could also be seen as differences in the density of summits, S_{ds}. This parameter decreased from 626 μm^{-2} on the latex coated surface to 238–358 μm^{-2} on the substrates with depositions of metal. From the topography images the metal grain size was also estimated for each metal-deposited sample. Overall, a thicker layer of metal deposition increased the lateral nano-grain size. This was more pronounced for Au, where the grain size increased from 11 nm (±3 nm) to 21 nm (±4 nm) for 2.5 nm and 5 nm thick samples, respectively. There was no clear increase in the size of the Ag grains, the average size increasing from 37 nm (±6 nm) to 44 nm (±17 nm). As can be seen from these values, the Ag particle aggregates were clearly larger than those of Au. Note that these values have not been corrected for tip geometry.

These observations indicate that Ag deposition covered more of the underlying latex nanostructure compared to Au deposition. Deposition of 2.5 nm Ag resulted in a smoothening of the surface. On the contrary, deposition of Au tended to increase the roughness. Due to the differences in the density and the particle size of Ag and Au, conceivably Ag vapor having less momentum encounters a higher resistance and preferentially stays on the latex surface, on the other hand Au might have partially penetrated in the latex film [15]. In either case, a thicker deposition of metal

Table 1
Compilation of surface analysis data listing peak positions and the atomic concentrations of the detected elements.

Ultra-thin Ag											
	Ag3p$^{1/2}$	Ag3p$^{3/2}$	O1s	Ag3d$^{3/2}$	Ag3d$^{5/2}$	Ca2p	C1s	%Ag	%C	%Ca	%O
1.Ag-2.5	604.1	573.4	531, 532.5	374.5	368.5	348.6	284.8, 286.1	28.8	59.9	0.58	10.6
2.Ag-2.5	604.1	573.4	531	374.5	368.5	–	284.8	38.6	50.9	0	10.4
3.Ag-2.5	604.1	573.4	531	374.5	368.5	–	284.8	40	49	0	10.2
1.Ag-5	604.1	573.4	531	374.4	368.4	348.6	284.8	36.4	57.5	0.5	5.6
2.Ag-5	604.1	573.4	531	374.4	368.4	348.6	284.8	35.6	58.7	0.3	5.4
3.Ag-5	604.1	573.4	531	374.4	368.4	–	284.8	37.8	56.4		5.6
Ultra-thin Au											
	Au4p$^{1/2}$	Au4p$^{3/2}$	O1s	Au4d$^{3/2}$	Au4d$^{5/2}$	Au4f$^{5/2}$	Au4f$^{7/2}$	C1s	%Au	%C	%O
1.Au-2.5	642.7	546.4	531.8	353.2	335.2	87.9	84.2	284.8,	29.1	62.8	8.1
2.Au-2.5	642.7	546.4	531.8	353.2	335.2	87.9	84.2	284.8	30.3	61	8.7
3.Au-2.5	642.7	546.4	531.8	353.2	335.2	87.9	84.2	284.8	32.3	59.7	7.9
1.Au-5	642.7	546.4	531.8	353.2	335.2	87.9	84.2	284.8	42.7	51.4	5.8
2.Au-5	642.7	546.4	531.8	353.2	335.2	87.9	84.2	284.8	40.9	52.4	6.5
3.Au-5	642.7	546.4	531.8	353.2	335.2	87.9	84.2	284.8	39.8	54	6.4

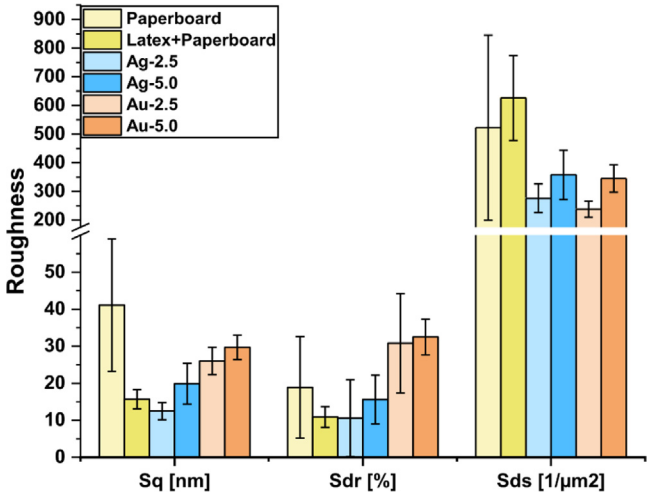

Fig. 2. Roughness characteristics (S_q, S_{dr} and S_{ds}) determined from 1 μm × 1 μm AFM images for all six (6) sample types. Error bars given are the standard deviation.

increased the fine structure and thereby the roughness, compared to thinner deposition.

3.2. X-ray photoelectron spectroscopy

The peak positions and the atomic concentrations of the detected elements from three different spots of ultra-thin silver and gold films are listed in Table 1. The measurements were performed on three different spots to study the surface homogeneity. The XPS results confirm that the grainy surface observed by AFM (Section 3.1) was indeed Ag and Au. A relatively high standard deviation of 6.1 in %Ag for Ag-2.5 was observed meaning that there were significant differences in the Ag coverage at different spots. Fig. 3 shows the survey and high-resolution spectra from three different spots on Ag-2.5 surfaces. Clear peaks associated with Ag, O and C could be seen in the survey spectra. At measuring spot 1 (1.Ag-2.5), a small amount of Ca was also detected. This likely originated from the paper substrate, calcite being a commonly used filler for paper. A closer look at the high-resolution spectra of Ag (Fig. 3) shows that there is no difference either in the peak position or peak shape for the Ag 3d peak from the three different spots. However, there is a small difference in the detected peak intensities. Based on literature, the peak positioned at 368.4 eV confirms the presence of Ag [19–21]. There might also be partial oxidation of silver and the presence of Ag_2O cannot be ruled out [20,21]. At spot 1 of Ag-2.5, the high-resolution spectra of C and O were slightly different in shape compared to spot 2 and 3. A second peak at higher binding energy of 286.1 eV and 532.5 eV was also observed for C1s and O1s, respectively. These peaks can be associated with the underlying latex coating and the paper substrate. Figure S2 shows the survey and high-resolution spectra from three different spots of Ag-5. Clear peaks associated with Ag, O and C can be seen in the survey spectra (Figure S2). A relatively low standard deviation of 1.1 in %Ag for Ag-5 was observed indicating that in this case, the Ag coverage at different spots was rather homogeneous. No differences were observed either in the peak positions or in the shapes of different identified peaks.

Both Au films, Au-2.5 and Au-5, were rather uniform in terms of metal coverage, seen as a low standard deviation of 1.6 and 1.4 %Au for Au-2.5 and Au-5, respectively. Similarly, no differences were observed in either the peak's positions or shapes for different identified peaks. As expected, a significantly higher amount of Au was detected for Au-5 compared to Au-2.5 (Table 1). The survey and high-resolution spectra of ultra-thin Au films are shown in Figure S3 and Figure S4.

3.3. Surface enhanced Raman spectroscopy

For SERS, paper is not the most desirable substrate due to background noise [22]. However, several studies have reported laboratory filter paper [23], inkjet printing paper [24], copier paper or chromatography paper-based SERS substrates [22]. In these studies, specifically designed nanoparticles have been directly deposited on the substrates in the form of dispersions or printing inks. Metallization of the substrates has also been performed using other methods such as vapor deposition [25]. The porosity and the surface roughness of the paper substrates has been utilized in producing the SERS substrates. However, these properties differ significantly within and among different grades of paper [26]. Therefore, different techniques such as soft lithography [27], electron beam lithography [28] etc. have been utilized to create precisely controlled nanostructures on flexible substrates for SERS applications. A comparison of nanostructured SERS substrate, the thickness of the metal film or particle dimensions and the resulting enhancement factor is presented in Table 2.

In this study, we report nanostructured latex coated paper substrates for prospective SERS application. A regulated surface nanostructure with controlled surface properties can be achieved by utilizing the latex-based coating reported here. SERS-active substrates are developed by depositing ultra-thin (2.5 nm and 5 nm) gold or silver layer.

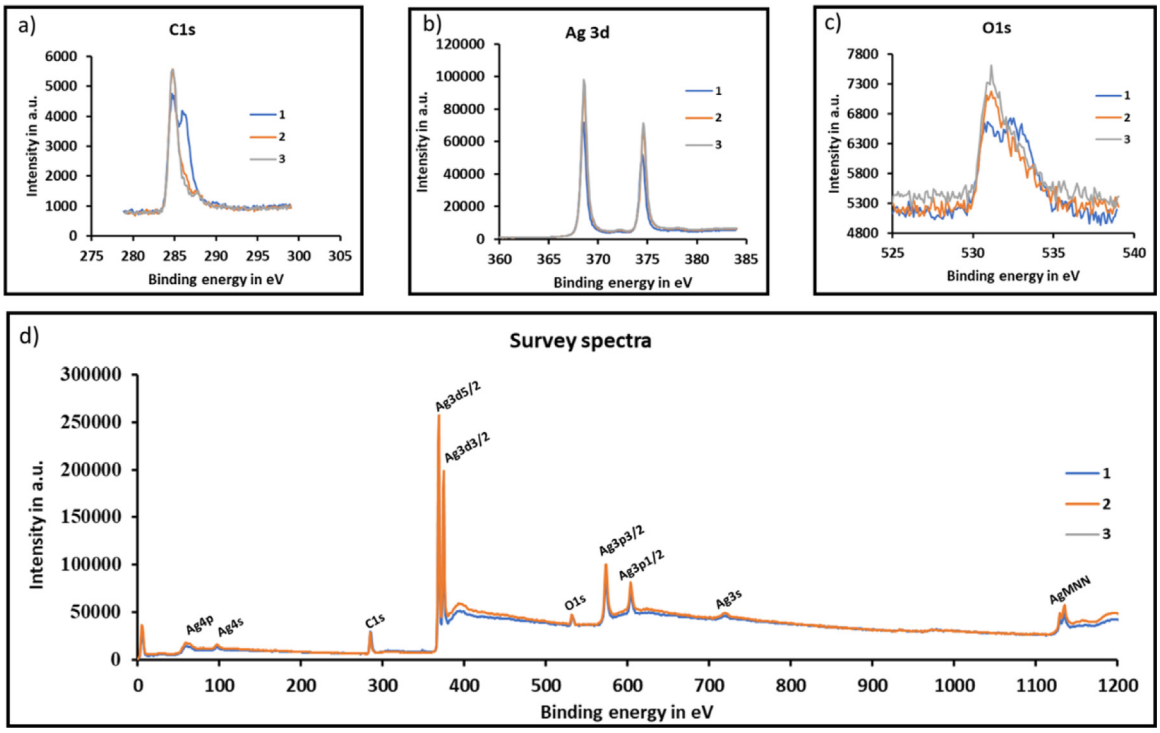

Fig. 3. Survey and high-resolution XPS spectra of C1s, Ag3d and O1s for Ag-2.5.

Table 2
A comparison of nanostructured SERS substrate, the thickness of the metal film or particle dimensions and the resulting enhancement factor.

Ref. No	Nanostructured SERS substrate	Thickness	Enhancement Factor	Concentration/ analyte
[22]	Inkjet-printing facilitated silver nanowires on paper substrate	Average diameter of nanowire is 70 ± 15 nm, and length of about 1–2 μm.	10^4	10^{-9}M/ rhodamine 6G
[29]	Ag-coated self-assembled polystyrene spheres	80, 120, 160 and 200 nm thick Ag films		10^{-9}M/ rhodamine 6G
[30]	Gold nanocones achieved by nanoimprint lithography on polycarbonate (PC) sheets	35 nm and 70 nm Au	10^5	10^{-4}M/ Crystal violet
[31]	Inkjet-printed silver particles on chromatography paper	200 nm Ag particles	10^5	
[18]	Au sputtering on the surface of the polymer nanostructure arrays	15 nm, 30 nm, 45 nm and 60 nm Au coating	10^7	10^{-6}M/ rhodamine 6G
[28]	Substrates Created via Electron Beam Lithography and physically vapor deposited silver	50 nm Ag		10^{-8}M/ Crystal violet
[27]	Ag layer on nanostructures created with soft lithography	60 nm Ag or 5 nm Cr, 60 nm Ag	10^6	10^{-6}M/ rhodamine 6G
[25]	Au sputtered filter paper	11.3 nm, 16.4 nm, 21.1 nm and 22.2 nm Au	10	10^{-6}M/ heavy metal ions
This study	Ultrathin physically vapor deposited Ag or Au film on nanostructured latex coated paper	2.5 nm and 5 nm Ag or Au	10^4	10^{-6}M/ rhodamine 6G/ Crystal violet

All four substrates were used for SERS analysis of different concentrations of crystal violet and rhodamine 6G, the test analytes. As seen in Fig. 4a and 4b, the four substrates show very similar SERS responses for the given instrumental settings. In Fig. 4a the SERS spectra display typical bands for crystal violet with the most prominent bands being the asymmetric ring stretching at around 1175 cm^{-1}, the ring stretching and CH bend at around 1391 cm^{-1} and the CNC bend at approx. 422 cm^{-1} and ring C–C stretch at 1617 cm^{-1} [32,33]. All spectra had a band at 1001 cm^{-1}, which is likely due to a contribution from polystyrene (PS) and acrylonitrile butadiene styrene (ABS) of the substrate coating [34]. This was confirmed by measurements on non-metal-coated substrate, i.e., paper–substrate coated with latex only (see Figure S5). Therefore, this band can potentially serve as an internal standard for all measurements. Thus, all spectra were normalized for the intensity of this band after background removal. Some spectra also showed a band at 1085 cm^{-1} that was likely resulting from CO_3^{-2} symmetric stretching. This could be due to pigment from the paper substrate [35]. All in all, as revealed by the raw spectra of all substrate measurements, background noise was negligible for both analytes on all substrates (see Figure S6).

Strong peaks centered around 612, 773, 1127, 1183, 1310, 1362 and 1510 cm^{-1} can be clearly seen from the rhodamine 6G

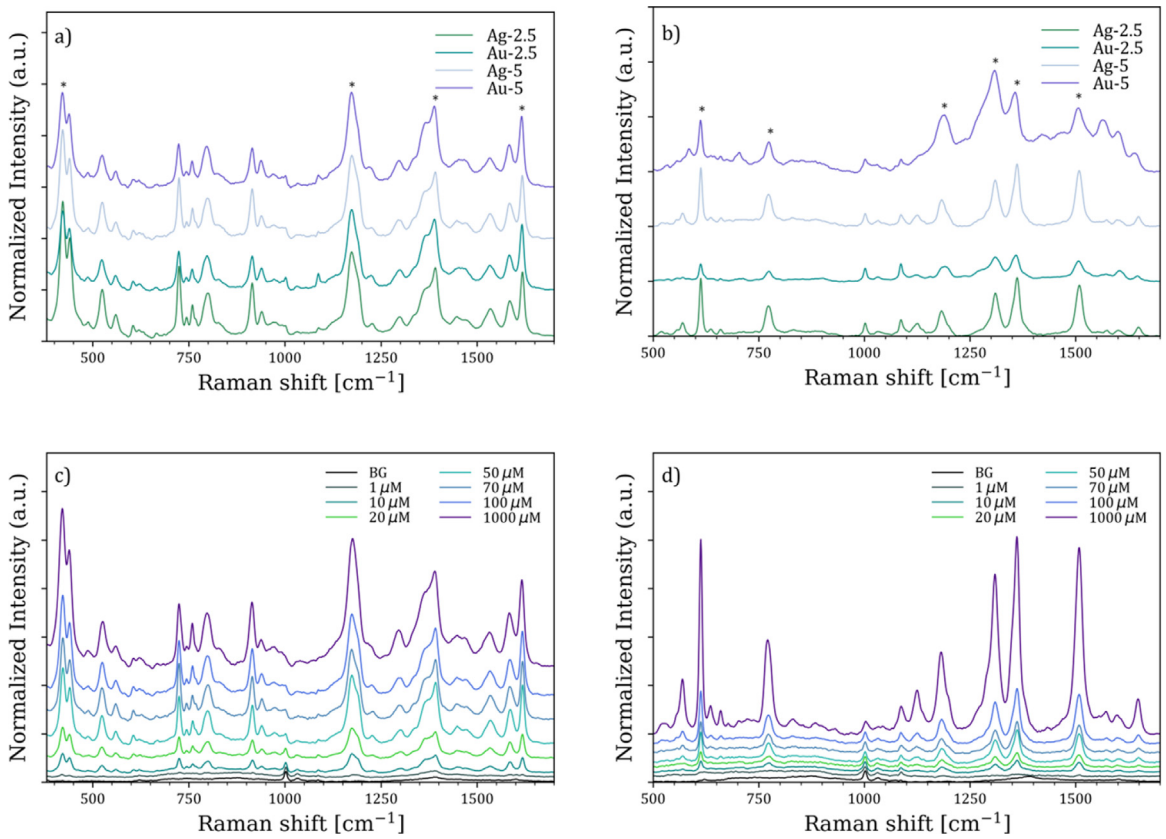

Fig. 4. Baseline-corrected and normalized average spectra of (a) crystal violet (100 μM) and (b) rhodamine 6G (100 μM) collected from substrates with 2.5 nm and 5.0 nm thick layer of Ag and Au, respectively. Baseline-corrected and normalized average spectra of (c) crystal violet and (d) rhodamine 6G in a concentration range from 1 to 1000 μM collected from a substrate with 5.0 nm thick layer of Ag. Assignments of marked peaks are provided in the text and SERS spectra of different substrates are offset for clarity.

spectra in Fig. 4b. These peaks are in agreement with the Raman signature of rhodamine 6G reported in the literature [36,37]. The Raman peak at 612 cm^{-1} is the C–C–C ring in-plane bending vibration. The peak at 773 cm^{-1} can be attributed to C–H out-of-plane bending vibration. The peaks at 1127 and 1183 cm^{-1} can be assigned to the C–H in-plane bending vibration. The Raman bands at 1310, 1362 and 1510 cm^{-1} are assigned to aromatic stretching vibrations [38,39].

Figs. 4c and 4d exemplify the SERS response for the Ag-5 substrate in a concentration range from 1 to 1000 μM of crystal violet and rhodamine 6G respectively, indicating a clear concentration dependence of the signal. As expected, the measured intensity was prone to certain replicate variation on all substrates. The relative standard deviations (RSD) for the four main bands of crystal violet were ranging from 1.5 to 21% after normalization, except for Au-2.5, which displayed RSDs around 39% (Table S2). It is important to note that this variation cannot only be attributed to the SERS effect as such. Likewise, RSD of around 9 to 22% was observed for rhodamine 6G for different substrates (Table S3). The laser spot of the Raman setup is very small, and since the "coffee ring effect" leads to an uneven distribution of the analyte molecules in the deposition area, sampling at different places may give rise to significant variations in intensity. In addition, the used Raman setup is sensitive to small differences in focusing between measurements. This also contributes significantly to intensity variations in the SERS spectra that is not fully corrected for by the normalization approach.

Analytical enhancement factors (AEFs) were calculated for all analyte/ substrate combinations. As reference spectra in these calculations, normal Raman spectra of crystal violet and rhodamine 6G obtained on a standard glass substrate (i.e. CaF_2) were used (see Figure S7). For all analyte/ substrate combinations, AEFs were mainly found in the region 10^3 – 10^4. However, when working on dried samples, concentrations are essentially unknown, and for the analysis of pure analytes on glass substrates, the coffee ring effect was especially pronounced. Thus, the AEFs reported here are highly uncertain and should be verified more thoroughly in future work. All in all, we expect that future work on optimization of the Raman setup and SERS measurements will lead to improvement in both reproducibility and enhancement effects, but the present study clearly shows the potential related to the paper-based substrates studied. Future studies on the normalization approach used in the current study, employing the intensity of the substrate-related band at 1001 cm^{-1}, will also be needed. If the paper substrates have "naturally occurring" internal standards that can be used for normalization, this is a clear benefit that should be exploited. Subsequently, this will depend on the reproducibility of the Raman band across different substrates.

4. Conclusions

An approach to fabricate low-cost, mass producible, flexible, disposable and environment friendly SERS-active substrate is reported here. The substrates were produced by roll-to-roll coating a two-component latex dispersion onto paperboard and IR drying. The SERS activity of the samples was obtained by depositing ultrathin layers of Ag or Au. The surface nanostructure was confirmed with AFM. XPS validated the successful deposition of the Ag or Au films. The utility of the substrates in SERS analysis was successfully studied with two analytes, crystal violet and rhodamine 6G. The observed background noise was negligible, and trace levels down to 10 μM of the tested analytes were

successfully detected. The developed substrate has the potential to be employed for swift and convenient testing of analytes for point-of-care, environmental as well as food quality control and safety applications.

Future work will focus on further improving the spatial reproducibility and the sensitivity of the developed substrate. We will study the effect of various surface nanostructures created by combining different ratios of the latex blend on the SERS signals.

CRediT authorship contribution statement

Emil Rosqvist: Methodology, Investigation, Writing – original draft, Writing – review & editing. **Ulrike Böcker:** Methodology, Investigation, Writing – review & editing. **Tina Gulin-Sarfraz:** Methodology, Investigation, Writing – review & editing. **Nils Kristian Afseth:** Conceptualization, Funding acquisition, Writing – review & editing. **Stiina Tolvanen:** Investigation, Writing – review & editing. **Jouko Peltonen:** Methodology, Funding acquisition, Writing – review & editing. **Jawad Sarfraz:** Conceptualization, Methodology, Investigation, Funding acquisition, Writing – original draft, Writing – review & editing.

Declaration of competing interest

The authors declare that they have no known competing financial interests or personal relationships that could have appeared to influence the work reported in this paper.

Data availability

Data will be made available on request.

Acknowledgments

We thank the Norwegian Fund for Research Fees for Agricultural Products (FFL) supporting the study through the projects, FutureFoodControl and PrecisionFoodProduction grant no. 314743 and 314111 respectively. Research council of Norway is also acknowledged for its financial support through project, NanoFunPack grant no 302243. We also want to acknowledge Jane and Aatos Erkko Foundation, Finland for funding the project ABC Health (Anti-Bacterial Channeling from Waste to Human Health). Tolvanen acknowledges Magnus Ehrnrooth Foundation, Finland for a personal grant.

Appendix A. Supplementary data

Supplementary material related to this article can be found online at https://doi.org/10.1016/j.nanoso.2023.100956.

References

[1] R. Pilot, SERS detection of food contaminants by means of portable Raman instruments, J. Raman Spectroscopy 49 (6) (2018) 954–981.
[2] S. Botti, S. Almaviva, L. Cantarini, A. Palucci, A. Puiu, A. Rufoloni, Trace level detection and identification of nitro-based explosives by surface-enhanced Raman spectroscopy, J. Raman Spectroscopy 44 (3) (2013) 463–468.
[3] Aılvarez-Puebla. RnA, Effects of the excitation wavelength on the SERS spectrum, J. Phys. Chem. Lett. 3 (7) (2012) 857–866.
[4] J. Zheng, L. He, Surface-enhanced Raman spectroscopy for the chemical analysis of food, Comprehensive Rev. Food Sci. Food Saf. 13 (3) (2014) 317–328.
[5] J. Chen, B. Shen, G. Qin, X. Hu, L. Qian, Z. Wang, et al., Fabrication of large-area, high-enhancement SERS substrates with tunable interparticle spacing and application in identifying microorganisms at the single cell level, J. Phys. Chem. C. 116 (5) (2012) 3320–3328.
[6] Y. Liu, Y. Zhang, M. Tardivel, M. Lequeux, X. Chen, W. Liu, et al., Evaluation of the reliability of six commercial SERS substrates, Plasmonics 15 (3) (2020) 743–752.
[7] A. Määttänen, P. Ihalainen, P. Pulkkinen, S. Wang, H. Tenhu, J. Peltonen, Inkjet-printed gold electrodes on paper characterization and functionalization, ACS Appl. Mater. Interfaces 4 (2) (2012) 955–964.
[8] P. Ihalainen, A. Määttänen, J. Järnström, D. Tobjörk, R. Österbacka, J. Peltonen, Influence of surface properties of coated papers on printed electronics, Ind. Eng. Chem. Res. 51 (17) (2012) 6025–6036.
[9] A. Määttänen, D. Fors, S. Wang, D. Valtakari, P. Ihalainen, J. Peltonen, Based planar reaction arrays for printed diagnostics, Sensors Actuators B Chem. 160 (1) (2011) 1404–1412.
[10] A. Määttänen, U. Vanamo, P. Ihalainen, P. Pulkkinen, H. Tenhu, J. Bobacka, et al., A low-cost paper-based inkjet-printed platform for electrochemical analyses, Sensors Actuators B Chem. 177 (2013) 153–162.
[11] E. Rosqvist, E. Niemelä, J. Frisk, H. Öblom, R. Koppolu, H. Abdelkader, et al., A low-cost paper-based platform for fast and reliable screening of cellular interactions with materials, J. Mater. Chem. B 8 (6) (2020) 1146–1156.
[12] H. Juvonen, A. Määttänen, P. Ihalainen, T. Viitala, J. Sarfraz, J. Peltonen, Enhanced protein adsorption and patterning on nanostructured latex-coated paper, Colloids Surf. B Biointerfaces 118 (2014) 261–269.
[13] P. San-Martin-Galindo, E. Rosqvist, S. Tolvanen, I. Miettinen, K. Savijoki, T.A. Nyman, et al., Modulation of virulence factors of staphylococcus aureus by nanostructured surfaces, Mater. Des. 208 (2021) 109879.
[14] J. Sarfraz, E. Rosqvist, P. Ihalainen, J. Peltonen, Electro-optical gas sensor consisting of nanostructured paper coating and an ultrathin sensing element, Chemosensors 7 (2) (2019) 23.
[15] P. Ihalainen, A. Määttänen, M. Pesonen, P. Sjöberg, J. Sarfraz, R. Österbacka, et al., Supported nanostructured ultrathin gold film electrodes–characterization and functionalization, Appl. Surf. Sci. 329 (2015) 321–329.
[16] E. Rosqvist, E. Niemelä, A.P. Venu, R. Kummala, P. Ihalainen, M. Toivakka, et al., Human dermal fibroblast proliferation controlled by surface roughness of two-component nanostructured latex polymer coatings, Colloids Surf. B Biointerfaces 174 (2019).
[17] C.A. Lieber, A. Mahadevan-Jansen, Automated method for subtraction of fluorescence from biological Raman spectra, Appl. Spectroscopy 57 (11) (2003) 1363–1367.
[18] C. Zhang, P. Yi, L. Peng, X. Lai, J. Chen, M. Huang, et al., Continuous fabrication of nanostructure arrays for flexible surface enhanced Raman scattering substrate, Sci. Rep. 7 (1) (2017) 1–9.
[19] M. Rom, M. Roubin, J.-P. Deloume, X-ray photoelectron emission studies of mixed selenides AgGaSe2 and Ag9GaSe6, J. Solid State Chem. 25 (1) (1978) 59–64.
[20] A.M. Ferraria, A.P. Carapeto, A.M.B. do Rego, X-ray photoelectron spectroscopy silver salts revisited, Vacuum 86 (12) (2012) 1988–1991.
[21] J. Chastain, R.C. King Jr., Handbook of X-ray photoelectron spectroscopy, Perkin-Elmer Corp. 40 (1992) 221.
[22] P. Joshi, V. Santhanam, Based SERS active substrates on demand, RSC Adv. 6 (72) (2016) 68545–68552.
[23] D. Mehn, C. Morasso, R. Vanna, M. Bedoni, D. Prosperi, F. Gramatica, Immobilised gold nanostars in a paper-based test system for surface-enhanced Raman spectroscopy, Vibrational Spectroscopy 68 (2013) 45–50.
[24] W.-J. Liao, P.K. Roy, S. Chattopadhyay, An ink-jet printed surface enhanced Raman scattering paper for food screening, RSC Adv. 4 (76) (2014) 40487–40493.
[25] Y. Song, Z. Ma, H. Fang, Q. Zhang, Q. Zhou, Z. Chen, et al., Au sputtered paper chromatography tandem raman platform for sensitive detection of heavy metal ions, ACS Sens. 5 (5) (2020) 1455–1464.
[26] D.-J. Lee, D.Y. Kim, Hydrophobic paper-based sers sensor using gold nanoparticles arranged on graphene oxide flakes, Sensors 19 (24) (2019) 5471.
[27] M. Kahraman, P. Daggumati, O. Kurtulus, E. Seker, S. Wachsmann-Hogiu, Fabrication and characterization of flexible and tunable plasmonic nanostructures, Sci. Rep. 3 (1) (2013) 1–9.
[28] N.A. Abu Hatab, J.M. Oran, M.J. Sepaniak, Surface-enhanced Raman spectroscopy substrates created via electron beam lithography and nanotransfer printing, ACS Nano. 2 (2) (2008) 377–385.
[29] L. Mikac, M. Ivanda, M. Gotić, V. Janicki, H. Zorc, T. Janči, et al., Surface-enhanced Raman spectroscopy substrate based on ag-coated self-assembled polystyrene spheres, J. Mol. Struct. 1146 (2017) 530–535.
[30] V. Suresh, L. Ding, A.B. Chew, F.L. Yap, Fabrication of large-area flexible SERS substrates by nanoimprint lithography, ACS Appl. Nano Mater. 1 (2) (2018) 886–893.
[31] W.W. Yu, I.M. White, Inkjet printed surface enhanced Raman spectroscopy array on cellulose paper, Anal. Chem. 82 (23) (2010) 9626–9630.
[32] M.V. Canamares, C. Chenal, R.L. Birke, J.R.D.F.T.. Lombardi, SERS and single-molecule SERS of crystal violet, J. Phys. Chem. C. 112 (51) (2008) 20295–20300.
[33] S. Fateixa, H.I. Nogueira, T. Trindade, Surface-enhanced Raman scattering spectral imaging for the attomolar range detection of crystal violet in contaminated water, ACS Omega 3 (4) (2018) 4331–4341.

[34] D. Reggio, D. Saviello, M. Lazzari, D. Iacopino, Characterization of contemporary and historical acrylonitrile butadiene styrene (ABS)-based objects pilot study for handheld Raman analysis in collections, Spectrochim. Acta Part A Mol. Biomol. Spectroscopy 242 (2020) 118733.
[35] F. Donnelly, F. Purcell-Milton, V. Framont, O. Cleary, P. Dunne, Y. Gun'ko, Synthesis of CaCO 3 nano-and micro-particles by dry ice carbonation, Chem. Commun. 53 (49) (2017) 6657–6660.
[36] Y. Ryu, G. Kang, C.-W. Lee, K. Kim, Porous metallic nanocone arrays for high-density SERS hot spots via solvent-assisted nanoimprint lithography of block copolymer, RSC Adv. 5 (93) (2015) 76085–76091.
[37] M. Zhang, A. Zhao, D. Li, H. Sun, D. Wang, H. Guo, et al., A simple and highly efficient route to the synthesis of NaLnF 4–Ag hybrid nanorice with excellent SERS performances, Analyst 137 (19) (2012) 4584–4592.
[38] P. Hildebrandt, M. Stockburger, Surface-enhanced resonance Raman spectroscopy of rhodamine 6G adsorbed on colloidal silver, J. Phys. Chem. 88 (24) (1984) 5935–5944.
[39] X.N. He, Y. Gao, M. Mahjouri-Samani, P. Black, J. Allen, M. Mitchell, et al., Surface-enhanced Raman spectroscopy using gold-coated horizontally aligned carbon nanotubes, Nanotechnology 23 (20) (2012) 205702.